IEEE Access
Multidisciplinary ⋮ Rapid Review ⋮ Open Access Journal

Received November 22, 2021, accepted December 5, 2021, date of publication December 22, 2021,
date of current version January 20, 2022.

Digital Object Identifier 10.1109/ACCESS.2021.3137747

On the Dynamic Response of the Ideal Paraboloidal Reflector

LEONARD T. BRUTON[1], (Life Fellow, IEEE), SANDUNI PREMARATNE[2], (Graduate Student Member, IEEE), AND PANAJOTIS AGATHOKLIS[2], (Life Senior Member, IEEE)

[1]Department of Electrical Engineering, University of Calgary, Calgary, AB T2N 1N4, Canada
[2]Department of Electrical and Computer Engineering, University of Victoria, Victoria, BC V8P 5C2, Canada

Corresponding author: Panajotis Agathoklis (panagath@ece.uvic.ca)

This work was supported in part by the Natural Sciences and Engineering Research Council of Canada, in part by the University of Victoria, and in part by the University of Calgary.

ABSTRACT The ideal paraboloidal reflector (IPR) is analyzed as a 4D spatio-temporal linear system having a dynamic focal plane response that is characterized by an idealized scalar Dirac plane-wave (PW) signal on the aperture. Using the same path-difference equations that are used for classical steady-state quasi-monochromatic (QMC) analysis, simple algebraic expressions are derived for the spatio-temporal focal plane response $h_{fp}(\boldsymbol{x}, ct)$ to the Dirac-PW. These expressions for $h_{fp}(\boldsymbol{x}, ct)$ are used to directly determine the focal plane response to far-field on-axis short-time transient signals, thereby avoiding the complexities of QMC-based methods for the analysis of such signals. The derived first-order approximation of $h_{fp}(\boldsymbol{x}, ct)$ describes its spatio-temporal region of support (ROS) and amplitude whereas the second-order approximation includes a further spatio-temporal distortion that is the dynamic equivalent of the Petzval aberration. Examples of the focal plane response to highly transient far-field pulses are described.

INDEX TERMS Broadband antennas, dynamic response of reflectors, paraboloid reflectors.

I. INTRODUCTION

The paraboloidal reflector is ubiquitous and has been very widely studied for at least 150 years. It is often employed to increase the intensity of a received aperture signal by bringing the signal into focus on the focal plane in the region of its focal point F. Such reflectors are also used to directionally transmit signals from the focal point into space via the aperture. Applications include the processing of photonic signals in such fields as radio astronomy, optical engineering, terrestrial telecommunications and satellite communications. Paraboloidal reflectors are also widely used for focusing and transmitting microwaves and airwaves in such fields as radar, audio, and ultrasonic signal processing [1].

In the following, we employ Huygens' Principle to derive several new useful algebraic approximations for the focal plane response $h_{fp}(\boldsymbol{x}, ct)$ to a Dirac-PW in the aperture and we show how these expressions may be employed to explain, determine, and predict the dynamic (transient and steady-state) response to general PWs received in the aperture from far-field on-axis sources. Our analysis makes the same path length assumptions about the geometry of the IPR, as shown in Fig.1, that are widely used for deriving the classical response to quasi-monochromatic (QMC) signals [2], [3].

Simple closed-form algebraic approximations for the region of support (ROS) of the 3D spatio-temporal function $h_{fp}(\boldsymbol{x}, ct)$ are derived and the shape of $h_{fp}(\boldsymbol{x}, ct)$ over that ROS is numerically confirmed for a wide range of focal lengths. Importantly, these approximations for $h_{fp}(\boldsymbol{x}, ct)$ may be used to determine the dynamic response of the IPR to general PW aperture signals, including short pulse-like transient signals, wavelets and other dynamic signals. These expressions for $h_{fp}(\boldsymbol{x}, ct)$ are simplified algebraically-equivalent versions of those in [4] and [5] and it is this simplicity that allows us to describe the behavior of $h_{fp}(\boldsymbol{x}, ct)$ over a wide range of focal lengths.

A. A BRIEF REVIEW OF PREVIOUS WORK

Classical multidimensional Fourier-based frequency-domain methods of analyzing the IPR [1]–[3] assume that the aperture input signal is quasi-monochromatic (QMC) and therefore closely approximated by a sinusoidal PW of temporal frequency ω_{t0} having an idealized 1D Fourier temporal-spectrum having Dirac support proportional to

The associate editor coordinating the review of this manuscript and approving it for publication was Kwok Chung.

$\delta(\omega_t - \omega_{t0}) + \delta(\omega_t + \omega_{t0})$. As described in [3], such QMC-based methods do not lend themselves to finding, explaining, or predicting the dynamic response of the IPR to important classes of non-QMC aperture signals, largely because conventional QMC-based analysis assumes that the IPR system has reached the periodic steady-state at a constant frequency ω_{t0}. This approach is often justified because of the prevalence in nature of QMC photonic signals and has yielded a very large body of QMC-based literature that is widely referenced in [1]–[3] and includes classical closed-form complex-valued algebraic transfer functions from the plane of the aperture to the focal plane, such as those due to Fraunhofer, Airy and Fresnel. QMC-based analysis has also yielded important classical algebraic approximations for the so-called aberrations of IPRs (and lenses), including both the Petzval de-focusing effect and off-axis coma distortion.

Further explanation of the use of QMC-based analysis for analyzing the dynamic performance of IPRs (and lenses) is summarized in Appendix A, essentially by assuming that the aperture signal and the corresponding focal plane response are approximated by the superposition of a large number of monochromatic signals via the multidimensional Fourier transform.

B. PREVIOUS DYNAMIC ANALYSIS OF THE IPR

The dynamic analysis of the IPR as a transmitting antenna has been studied for the case of electromagnetic short-pulses and later, in a series of related publications [6]–[10]. In this body of work, the source is at the focal point of the IPR and closed-form expressions are derived for the electric and magnetic fields radiated by the IPR to locations in space. By assuming a Dirac source function at the focal point, these pioneering works lead to polynomial expressions for the electric and magnetic impulse responses of the IPR in the direction from the focal point to a location in free space. Importantly, they exploit the fact that the impulse response fully characterizes the response of the IPR system to general short-time dynamic transmitted signals, including wave propagation from the focal point to the reflector. As an example, the radiated response to a short Gaussian pulse at the focal point has been reported. This previous work differs from this contribution in several ways. First, we study the dynamic response of the IPR as a *receiver* rather than as a transmitter: that is, in the reverse direction whereby the received input signal is a PW on the aperture and the output of the IPR system is the focal plane onto which the received signal is reflected. The IPR receiver is considered as a stand-alone spatio-temporal 4D linear system that does not inherently depend on the scalar propagation equation, such as the Rayleigh-Sommerfeld model, that may subsequently be required to evaluate the focal plane response due to a far-field source.

In this contribution and following [4], [5], the focal plane response to a *general* received dynamic aperture PW is obtained from $h_{fp}(\boldsymbol{x}, ct)$ via 1D temporal convolution, essentially determining the general received aperture PW as the superposition of elemental delayed-Dirac functions. In contrast, QMC-based analysis forms the general aperture PW as a superposition of elemental monochromatic signals, as further explained in Appendix A. Thus, the approach used in this paper is based on the frequency-time dual of QMC-based analysis: that is, by assuming idealized Dirac support in the time domain rather than in the frequency domain.

In the following, the results in [4] and [5] are improved upon and extended in the following ways. First, new approximate and much-simplified closed-form algebraic expressions for $h_{fp}(\boldsymbol{x}, ct)$ are derived. Second, the hypothesis in [4] and [5] that the Petzval aberration applies with high accuracy to *dynamic* responses is confirmed. Third, temporal convolutions are described that explain and confirm how the IPR responds to highly transient electric field sources in the far field of the IPR. Throughout, numerical verifications are presented that confirm the accuracy of these new expressions for $h_{fp}(\boldsymbol{x}, ct)$ over a wide range of focal lengths.

II. THE FOCAL PLANE RESPONSE OF THE IDEAL PARABOLIC REFLECTOR TO THE DIRAC-PW APERTURE SIGNAL

The surface of the *ideal* paraboloidal reflector (IPR) is illustrated in Fig. 1 where the 3D spatial co-ordinates $\boldsymbol{x} \equiv (x_1, x_2, x_3)$ are identified and where the disc-shaped aperture and the focal plane are in parallel. Relevant angles and path lengths are also shown in Fig.1.

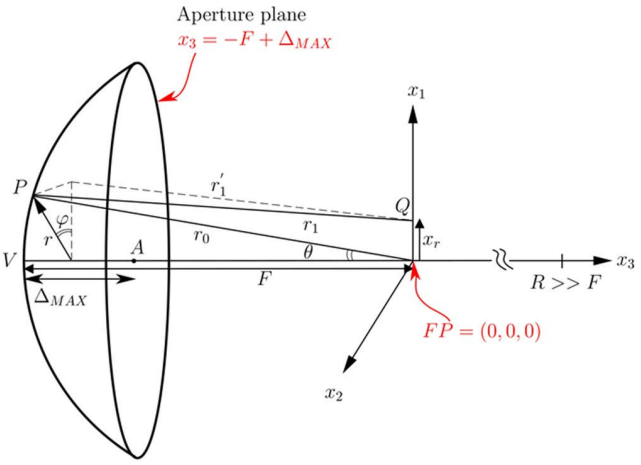

FIGURE 1. The paraboloidal reflector.

The aperture plane is given by $x_3 = -F + \Delta_{max}$ and $x_3 < 0$, the on-axis focal point F is at $\boldsymbol{x} \equiv (0, 0, 0)$, the vertex V is at $\boldsymbol{x} \equiv (0, 0, -F)$, P is any point on the paraboloid and the focal plane is given by $x_3 = 0$. In this contribution, we assume that the source signal is on-axis in the far-field of the IPR at $\boldsymbol{x} \equiv (0, 0, R)$ such that $R \gg F$, implying that the signal received in the aperture disc lies approximately on a PW. In the following, we characterize the dynamic focal plane response $h_{fp}(\boldsymbol{x}, ct)$ of the IPR to an idealized scalar Dirac plane-wave (PW) signal that is received on the aperture plane at time instant $t = -(F - \Delta_{max})/c$ and therefore at

the vertex V at time instant $t = -F/c$ from which it reaches the focal point (FP) at $t = 0$.

The Dirac-PW aperture signal is defined as follows:

$$\mathbf{Dirac}_{aper}(x, ct) = \frac{1}{c}\delta(ct - \Delta_{max} + F) \quad \text{for} \begin{cases} x_r \equiv \sqrt{(x_1^2 + x_2^2)} \le D/2, \\ x_3 = -F + \Delta_{max} \end{cases}$$
$$\mathbf{Dirac}_{aper}(x, ct) = 0 \quad otherwise \tag{1}$$

where $\Delta_{max} + F$ is the distance along the path $\overline{AVF}$ shown in Fig.1, implying that this instantaneous signal is reflected from the vertex V at the instant $t = -F/c$ and therefore is incident at the focal point FP from *all* locations P at the instant $t = 0$. For all $x_r > 0$, wave fronts are received at the focal plane over a *continuous* range of times as determined in the following analysis. This temporal dilation is a direct consequence of the spatial compression from aperture to focal plane: that is, of spatial focusing.

In Appendix B, we employ Huygens' principle to determine the double-integral that expresses the focal plane response $h_{fp\_exact}(\boldsymbol{x}, ct)$ without any approximations beyond that implied by the spectral validity of this principle [2]. We note that Huygens' principle is invalid for spectral temporal-frequency components ω_t of the received signal that do not satisfy the inequality $2\pi/\omega_t c \ll D$; equivalently, the corresponding largest spectral wavelength λ_t of the received dynamic signal must be at least an order of magnitude less than the diameter of the dish and of all path lengths. In Appendix B, we use a number of well-known path length approximations [1]–[3] to significantly reduce the algebraic complexity of $h_{fp\_exact}(\boldsymbol{x}, ct)$. The first-order approximation $h_{fp1}(\boldsymbol{x}, ct)$ and the second-order approximation $h_{fp2}(\boldsymbol{x}, ct)$ may be considered as time-delay versions of the phase-shift approximations used in classical QMC-based analysis.

A. THE SEMI-ELLIPTICAL FOCAL PLANE RESPONSE EMPLOYING THE FIRST-ORDER APPROXIMATION $h_{fp1}(\boldsymbol{x}, ct)$

In Appendix C1, the first-order path difference assumption is employed to prove that the focal plane response is given by:

$$h_{fp1}(\boldsymbol{x_r}, ct) \approx \frac{2}{x_r} tan^{-1}\left(\psi(x_r, t)\frac{8}{16\left(\frac{F}{D}\right) - \left(\frac{D}{F}\right)}\right) \quad for\ 0 < \psi(x_r t) < 1, \quad F \ge D/4$$
$$h_{fp1}(\boldsymbol{x_r}, ct) \approx otherwise \tag{2}$$

where

$$x_r \equiv \sqrt{x_1^2 + x_2^2}$$
$$\Psi(x_r, t) = \sqrt{\left(1 - \left(\frac{ct}{x_r\, sin\ (\theta_{max})}\right)^2\right)} \tag{3}$$

and

$$\theta_{max} = tan^{-1}\left(\frac{8FD}{16F^2 - D^2}\right) \tag{4}$$

The 3D focal plane response $h_{fp1}(x_r, ct)$ represents the 4D function $h_{fp1}(\boldsymbol{x}, ct)$ on the focal plane, i.e., for $\boldsymbol{x} = (x_1, x_2, 0)$. To our knowledge, (2) is a new result where the function $\psi(x_r, t)$ plays a key role in determining both the ROS and the semi elliptical shape of $h_{fp1}(x_r, ct)$ and is therefore defined here as the *dynamic generation function* (*dgf*). The 3D spatio-temporal ROS of $h_{fp1}(x_r, ct)$ that is obtained from $0 < \psi(x_r, t) < 1$, is equivalent to the ROS in C7 and it is shown in Fig. 2(a). In Fig. 2(a) the value of $h_{fp1}(x_r, ct)$ is also illustrated for three values of x_r.

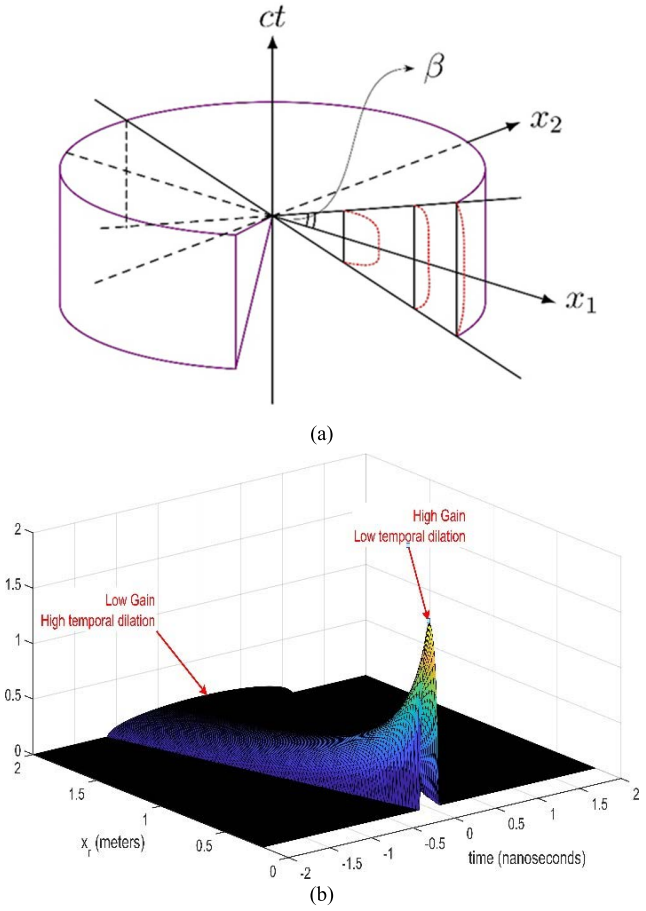

FIGURE 2. **(a) The 3D spatio-temporal ROS of $h_{fp1}(x_r, ct)$ is the exterior of a wide angle cone, as shown, where $\beta = tan^{-1}(\theta_{max})$. The value of $h_{fp1}(x_r, ct)$ is indicated for three value of x_r by the red curves. (b). $h_{fp1}(x_r, ct)$ for $F = 15m$, $D = 6.75m$ showing the role of the decaying semi-elliptic pulse as x_r increases.**

The shape of $h_{fp1}x_r(, ct)$ is also determined by $\psi(x_r, t)$ which represents a semi-ellipse for constant x_r. As x_r increases from 0, the long axis of the ellipse is moving from the temporal direction to the spatial direction. In Fig2(b) we show $h_{fp1}(x_r, ct)$ for the Square Kilometer Array (SKA) IPR paraboloid [11], [12] with $F = 15m$, $D = 6.7\ m$

as a continuous function of space-time, thereby quantifying the time-dilation and confirming the asymptotic decrease of amplitude with increasing distance x_r and the corresponding asymptotic increase in its duration the decaying semi-elliptic pulse as x_r increases.

Both the tangent and inverse tangent operations in (2) may be neglected for F/D ratios greater than about unity, yielding the particularly simple further approximation

$$h_{fp1}(x_r, ct) \approx \frac{2\theta_{max}\psi(x_r, t)}{x_r}, \quad for\ 0 < \psi(x_r, t) < 1F > D/4$$
$$h_{fp1}(x_r, ct) \approx 0 \quad otherwise \tag{5}$$

B. ON THE ACCURACY OF THE SIMPLIFIED EXPRESSION IN EQUATION 5

The especially simple approximation of equation (5) is valid over a wide range of F/D ratios. It follows from equation (4) that $F/D \rightarrow \infty$ implies that $\theta_{MAX} \rightarrow 0$ and therefore $h_{fp1}(x_r, ct)$ is given by equation (5). In Fig. 3 we show the limitation of equation (5) by displaying a slice through $h_{fp1}(x_r, ct)$ at $x_r = 1\ m$ for various low-valued F/D ratios, ranging from 0.8 to as low as 0.3. Clearly, the modifying effect of the tangent and inverse tangent operations in equation (2) is to perturb the semi-elliptical shape of $h_{fp1}(x_r, ct)$ as shown for $F/D = 0.3$, 0.5 and 0.8. A similar result is obtained for other constant x_r slices of $h_{fp1}(x_r, ct)$.

III. THE SECOND ORDER PETZVAL ABERRATION AND EXACT HUYGENS ANALYSIS

In Appendix C2, the second-order path difference assumption is employed to prove that the focal plane response is given by:

$$\boldsymbol{h_{fp2}(x_r, ct)} \approx \frac{2}{x_r} tan^{-1}\left(\sqrt{1-\left(\frac{ct-\frac{x_r^2}{2F}}{x_r\, sin\,\theta_{MAX}}\right)^2}\ \frac{8}{16\left(\frac{F}{D}\right)-\left(\frac{D}{F}\right)}\right)$$
$$for\ \left|\frac{ct-\frac{x_r^2}{2F}}{x_r\, \sin\theta_{MAX}}\right| < 1, \quad F \geq D/4$$
$$\boldsymbol{h_{fp2}(x_r, ct)} \approx 0 \quad \text{otherwise} \tag{6}$$

Relative to $h_{fp1}(\boldsymbol{x_r}, ct)$, this second-order term $x_r^2/2F$ introduces a delay of $x_r^2/2Fc$ seconds *without otherwise altering its dgf-determined shape.* This is shown in Fig.4 where the exact focal plane response $h_{fp\_exact}(x_r, ct)$ (computed using the numerical evaluation of (B.1) discussed in the next section) is compared with $h_{fp1}(x_r, ct)$ and $h_{fp2}(x_r, ct)$ for $F = 6.75m$, $D = 15m$ *and* $x_r = 1m$.

It can be seen in Fig. 4 that the delay between $h_{fp1}(x_r, ct)$ and $h_{fp2}(x_r, ct)$ for this case is, as expected, about 0.24 nanoseconds. The exact solution $h_{fp\_exact}(x_r, ct)$ is in very good agreement with $h_{fp2}(x_r, ct)$, any small differences representing the effect of third and higher order terms.

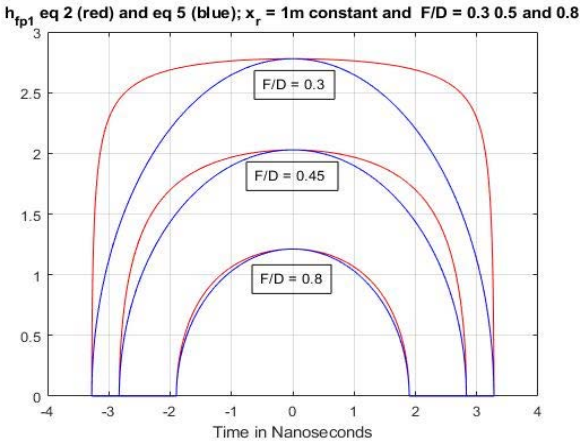

FIGURE 3. The focal plane Dirac-PW response $h_{fp1}(1, ct)$ for $F/D = 0.3$, 0.5 and 0.8 confirming the requirement to use equation (5) instead of equation (2) for $F/D < 1$.

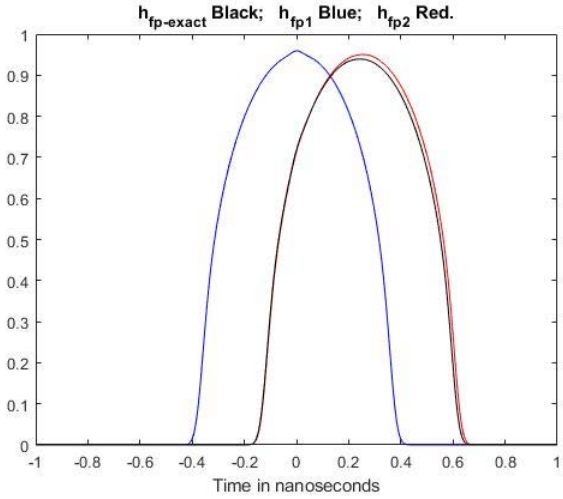

FIGURE 4. The exact Huygens' solution $h_{fp\_exact}(x_r, ct)$ in Appendix B, eq. (B.1), the first-order approximation $h_{fp1}(x_r, ct)$ in (2) and the second-order approximation $h_{fp2}(x_r, ct)$ in (6); $F = 6.75m$, $D = 15m$ and $x_r = 1m$.

It is suggested and partly explained in [4] and [5] that this second-order approximation corresponds to the *dynamic version of the QMC-derived Petzval aberration*. This is confirmed in Fig. 5 where the ROS is upwardly skewed onto a paraboloid by the second-order term. The dotted-blue parabolic 3D surface given by $ct = x_r^2/2F$ implies *late* arrival by time $x_r^2/2Fc$ *relative to the time of arrival at the focal plane*. For the on-axis case, this late arrival closely corresponds to the non-physical Petzval paraboloidal surface $x_3 \approx ct = x_r^2/2F = \sqrt{x_1^2 + x_2^2}/2F$ obtained by rotating the dotted blue curve in Fig. 5 by 2π about the ct axis. This Petzval surface in $\boldsymbol{x}$ has its vertex at the focal point, $\boldsymbol{x} = (0, 0, 0)$, a focal length of $F/2$, is curved outwards from the reflector and its focal point is at [1] $\boldsymbol{x} = (0, 0, F/2)$.

[1] *The suggestion in* [5] *showed the Petzval surface for a lens rather than a reflector. For a lens, the curves in Fig. 5 are skewed downwards instead of upwards.*

The *entire* 3D spatial ROS of $h_{fp2}(x_r, ct)$ is the volume in (x_1, x_2, ct) that lies between the two surfaces obtained by similarly rotating the red curves by 2π in Fig. 5

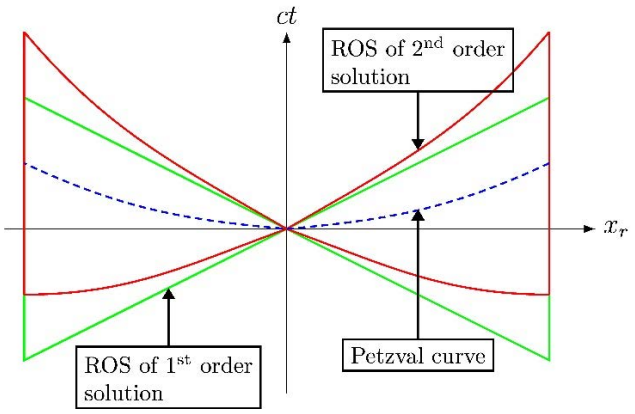

FIGURE 5. Region of support of h_{fp} for first-order and second order approximation. The 3D regions of support are obtained by 2D rotation by 2π around the ct axis.

We conclude that, as for QMC signals, the second-order response *to dynamic signals* is more sharply represented on the Petzval paraboloidal surface than on the focal plane. Consequently, *Petzval-curved dishes may be preferable than a plane in applications involving short transient dynamic signals*. As a numerical example of the extent of the Petzval correction, for a focal length of 6.75 m, to retain sharp dynamic images out to a distance of $x_r = 1$ meter from the focal point the required physically-curved Petzval surface is a distance of 7.4 cm from the focal plane. We note that the location of the Petzval surface does not depend on diameter D or speed c.

A. EXACT HUYGENS' ANALYSIS

In order to evaluate the *accuracy* of the above first-order and second-order path difference approximations, we have numerically evaluated the exact Huygens' expression in (B.1).

It should be noted that for this approach is limited by the fact that Huyghen's Principle is a valid approximation for both the diameter D of the dish and the focal length F requires that both are at least an order of magnitude larger than the longest significant wavelength of the signal Numerical evaluation of (B.1) is non-trivial because the delayed Dirac function in the integrand of (B.1) will, in general, be zero at the discrete numerical samples of $h_{fp}(x_r, ct)$ and the instants when it is non-zero will be between those samples. Thus, temporal resolution is a serious technical challenge that will always yield inexact solutions. Accordingly, we have separately developed a numerical integration program in MATLAB to approximate (B.1) to arbitrary spatial and temporal precision. For brevity, the details of the program are omitted.

This program has been used to compute $h_{fp\_exact}(x_r, ct)$, the exact solution using (B.1), which is used in Fig. 4. to evaluate the accuracy of the 3 focal plane responses for the SKA IPR: they are the exact Huygens solution in (B.1), the first-order approximation in (2) and the second-order approximation in (6), shown in Fig. 4. The results, as discussed in the previous section, are observed to be in very good agreement.

IV. ON $r_{fp}(x_r, ct)$, THE FOCAL PLANE RESPONSE TO FAR FIELD SOURCES

We have so far assumed the existence of a PW on the aperture without considering the wave propagation equation that models the propagation from the far field source to the aperture. Following [3], we model the propagation of the PW from the far-field employing the scalar wave Rayleigh-Sommerfeld equation applied to photonic propagation at speed c. In that case, let the far-field photonic source be written $u_{FF}(\boldsymbol{x}, ct) = u_{FF}(0, 0, R, ct)$, $R \gg F$ resulting in a propagation-delayed and significantly attenuated aperture signal [3] of the form

$$\boldsymbol{u_{aperture}}(x, \boldsymbol{ct}) = \frac{1}{\boldsymbol{R_s c}} \frac{\boldsymbol{d}}{\boldsymbol{dt}} [\boldsymbol{u_{FF}}(x, \boldsymbol{ct} + \boldsymbol{R_s})] \tag{7}$$

where, from Fig.1, $R_s = R + F - \Delta_{MAX}$ and is the path distance from the far-field spatial point source to the aperture. The response on the focal plane $r_{fp}(x_r, ct)$ *to this far-field excitation* $u_{FF}(\boldsymbol{x}, ct + R_s)$ is therefore given by,

$$\begin{aligned} &\boldsymbol{r_{fp}}(\boldsymbol{x_r}, \boldsymbol{ct}) \\ &= \frac{1}{\boldsymbol{R_s c}} \Big[\boldsymbol{h_{fp}}(\boldsymbol{x_r}, \boldsymbol{ct} - \boldsymbol{R_s}) \\ &\quad * \frac{\boldsymbol{d}}{\boldsymbol{dt}} [\boldsymbol{u_{FF}}(\boldsymbol{0}, \boldsymbol{0}, \boldsymbol{R_s}, \boldsymbol{ct} - \boldsymbol{R_s})] \Big] \end{aligned} \tag{8}$$

where $*$ denotes 1D convolution with respect to ct. (8) allows the focal plane temporal response to be determined as a function of distance x_r from the focal point. It is emphasized that this equation assumes that Huygens' Principle in (1) is accurate at all temporal frequencies and yet this is only a valid assumption for spectral components of the source signal that have corresponding wavelengths that are at least an order of magnitude smaller than the diameter D and the path lengths in Fig.1. QMC-based analysis typically makes the same assumptions about the wavelength of the chromatic signal [2], [3].

It is noted that the derivative term in (7) implies that the temporal average of $r_{fp}(x_r, ct)$ is zero.

V. SOME EXAMPLES OF RESPONSES TO DYNAMIC FAR-FIELD SOURCES

A. EXAMPLE 1: FOCAL PLANE RESPONSE TO A FAST GAUSSIAN TRANSIENT BURST IN THE FAR-FIELD

Consider the transient far-field Gaussian pulse $u_{FF}(0, 0, R, ct)$ shown in Fig. 6(a) along with its temporal derivative in Fig. 6(b), where both pulses have an effective duration of approximately 4 nanoseconds.

The purpose of this example is to demonstrate the usefulness of $h_{fp1}(\boldsymbol{x_r}, ct)$ for directly determining the focal plane response of the IPR to short duration pulses of this type. Considering again the SKA paraboloid with $F = 6.75m$, $D = 15m$, we evaluate (8), i.e., the temporal convolution between

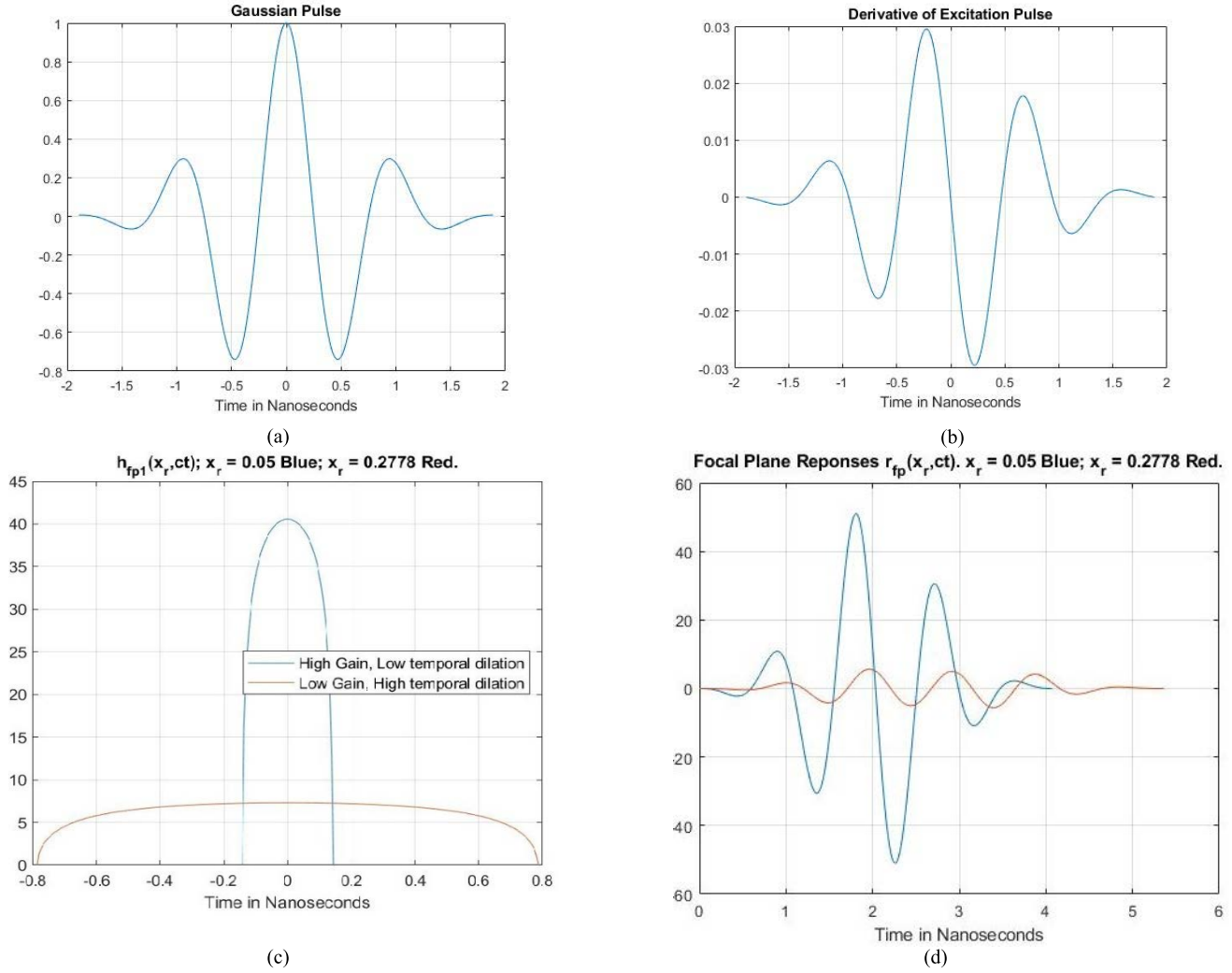

FIGURE 6. (a). Example 1: Far-field Gaussian impulse as the input signal. (b). Example 1: The derivative of the impulse signal. (c). Example 1: $h_{fp1}(x_r, ct)$ for $x_r = 0.05$ m and $x_r = 0.2778$ m. (d). Example 1: Focal plane responses $r_{fp}(x_r, ct)$ for $x_r = 0.05$ m and $x_r = 0.2778$ m.

$h_{fp1}(\boldsymbol{x_r}, ct)$ and the aperture signal shown in Fig. 6(b), for the two values $x_r = 0.05m$ and 0.2278m. For these values of x_r, (8) yields the corresponding two focal plane responses $r_{fp}(x_r, ct)$ shown in Fig. 6(d) where the propagation delay has been ignored by centering the responses about the time origin. These responses are easily explained. For $x_r = 0.05$m, the location is sufficiently close to the focal point so that the duration of $u_{FF}(0, 0, R, ct)$ is much larger than that of $h_{fp1}(0.05, ct)$ (shown as the blue curve in in Fig. 6(c)). This results in a $r_{fp}(x_r, ct)$ (shown as the blue curve in Fig. 6(d)) with a high amplitude and a shape which is close to that of the received signal in the aperture.

At $x_r = 0.2778$m, this relative increase in distance from the focal point yields a function $h_{fp1}(0.2778, ct)$ (shown as the red curve in Fig. 6(c)) that is of significantly larger duration and lower amplitude than the received aperture signal. This is causing the response $r_{fp}(0.2778, ct)$ (shown as the red curve in Fig. 6(d)) to be attenuated and spatially smeared by $h_{fp1}(0.2778, ct)$ that it fails to significantly respond to the received aperture signal and consequently consists in large part of the transient behavior of the IPR.

B. EXAMPLE 2: A SWITCHED-ON AND SWITCHED-OFF SINUSOIDAL FAR-FIELD EXCITATION AND THE QMC-BASED STEADY-STATE AIRY DISC

Consider the IPR with the following parameters: $D = 15m, F = 6.75m, c = 3 \times 10^8\ m/s$. Let the IPR be excited by a *far-field* switched-on/switched-off sinusoidal PW signal given by

$$\begin{aligned} \boldsymbol{e_{FF}}(\boldsymbol{x}, ct) &= \boldsymbol{e_{FF}}(0, 0, R, ct) \\ &\equiv (\boldsymbol{u}(\boldsymbol{ct}) - \boldsymbol{u}(\boldsymbol{ct} - \boldsymbol{cT}))\, \boldsymbol{sin}\left(\boldsymbol{\omega_{0,ct}} ct\right), \\ \boldsymbol{\omega_{0,ct}} &= \boldsymbol{\omega_{0,t}}/\boldsymbol{c} \end{aligned} \tag{9}$$

implying that the temporal frequency is given in Hz by $f_{0,t} = \omega_{0,t}/2\pi$ and that the sinusoid is switched on at $t = 0$ and off T seconds later. In this example we use $f_{0,t} = 4.41\ GHz$ and $T = 0.908$ *nanoseconds*. Neglecting the attenuation from the

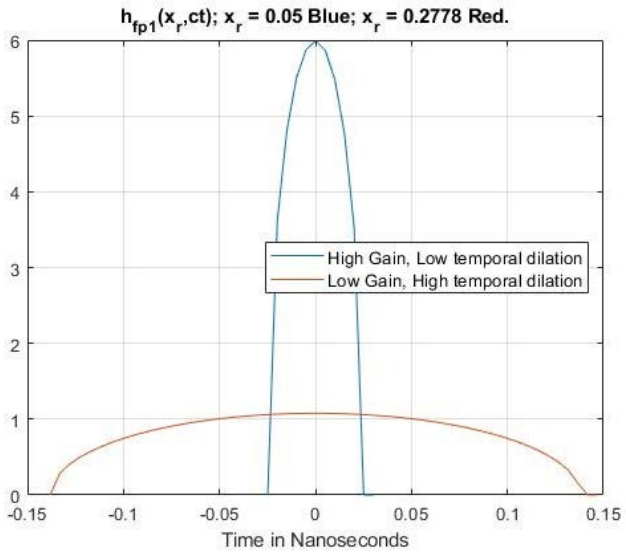

(a)

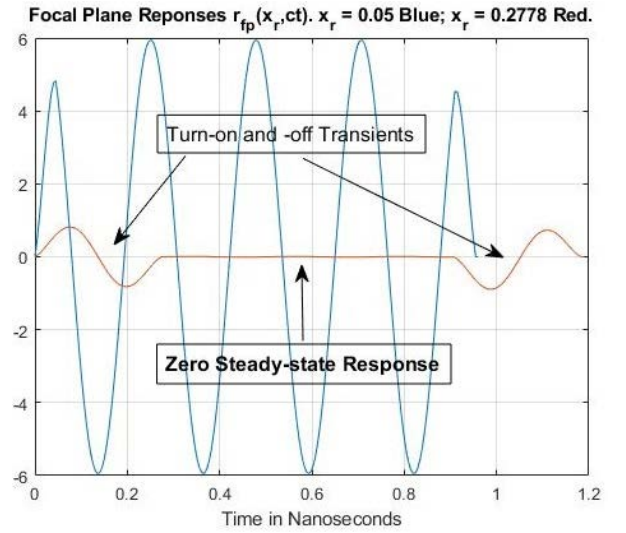

(b)

FIGURE 7. (a). Example 2: $h_{fp1}(x_r, ct)$ for $x_r = 0.05$ m and $x_r = 0.2778$ m. (b). Example 2: Focal plane responses $r_{fp}(x_r, ct)$ for $x_r = 0.05$ m and $x_r = 0.2778$ m.

far-field to the aperture plane, it follows from (8) and (9) that the focal plane response is proportional to

$$r_{fp}(x_r, ct) = \left[h_{fp}(x_r, ct) * \frac{d}{dt}\left[(u(ct) - u(ct - cT))\, sin\left(\omega_{0,ct} ct\right)\right]\right] \tag{10}$$

and thus to

$$r_{fp}(x_r, ct) = \left[h_{fp}(x_r, ct) * \left[(u(ct) - u(ct - cT))\, cos\left(\omega_{0,ct} ct\right)\right]\right]$$

C. ZERO-VALUED AIRY CIRCLE AT STEADY STATE, $x_r = 0.2778m$

For $f_{0,t} = 4.41$ GHz and $T \to \infty$ in equation (9), the resultant classical QMC-based *steady-state* focal plane response $r_{fp}(x_r, ct)$ is almost exactly zero at $x_r = 0.2778$ m. This corresponds to a zero-valued circle on the Airy disc [3]. However, the *complete* dynamic response $r_{fp}(x_r, ct)$ of equation (10) for finite T is not zero because it includes the turn-on and turn-off transients as shown in the red curve in Fig 7(b) for $T = 0.908$ nanoseconds. The duration of these transients is 0.3 nanoseconds, exactly the duration of the corresponding $h_{fp1}(x_r, ct)$ as shown with the red curve in Fig. 7(a).

D. NON-ZERO-VALUED AIRY STEADY-STATE, $x_r = 0.05m$

Consider now the same signal as in the previous case of this example, but at a location that is much closer to the focal point and is given by , $x_r = 0.05m$. For this case $h_{fp1}(x_r, ct)$ is given with the blue curve in Fig. 7(a) and clearly, $h_{fp1}(x_r, ct)$ is of significantly shorter duration and higher gain than in the previous case. Accordingly, the transient response $r_{fp}(x_r, ct)$ for $x_r = 0.05$ given with the blue curve in Fig. 7(b) is of shorter duration (about 0.05 nanoseconds) and the steady-state response is now non-zero, as would be expected from the classic QMC approach.

Remark: The proposed general *dynamic* theory describes the complete response (transient and steady-state) and thereby includes the quasi-monochromatic (QMC) *steady-state* behavior of the ideal parabolic reflector *as a special case*. The theoretical results of the proposed approach are entirely consistent with both the theoretical and experimental behavior of QMC steady state results and they yield the classical Airy disc.

VI. CONCLUSION

New algebraic expressions for the focal plane response $h_{fp}(x_r, ct)$ of the IPR to a Dirac-PW in the aperture have been derived from Huygens's Principle,. These expressions reveal that $h_{fp}(x_r, ct)$ is characterized by a semi-elliptic dynamic generation function (*dgf*) that yields a semi-elliptical focal plane response to the Dirac-PW aperture excitation. The shape and 2D spatio-temporal ROS of $h_{fp}(x_r, ct)$ have been derived and explained. The path length approximations used are those widely employed for classical QMC-based Fourier analysis. The second order approximation obtained by including the additional term $x_r^2/2F$ in the path difference approximation, confirmed and quantified the observation in [4] and [5] that the signal received on the Petzval paraboloid corrects the corresponding aberration delay of the *dynamic* focal plane response. These new results are algebraically equivalent to those first published in [4], [5] for $h_{fp1}(x_r, ct)$ but are far more algebraically simple.

Further, by temporally convolving the Dirac PW response $h_{fp}(x_r, ct)$ with the attenuated and delayed time-derivative of the far-field source, the full dynamic focal plane response to general on-axis far-field signals is obtained for photonic signals. Two examples have been presented to illustrate this.

The above analysis is the frequency-time dual of classical QMC-based analysis, where the latter assumes Dirac support in the frequency domain whereas we assume Dirac

support in the time domain. The proposed general *dynamic* theory describes the complete response (transient and steady-state) and thereby includes the quasi-monochromatic (QMC) *steady-state* behavior of the ideal parabolic reflector *as a special case.*

APPENDIX A
REVIEW OF QMC-BASED FOURIER ANALYSIS FOR DYNAMIC PW SIGNALS

In the general case, we are concerned with 4D spatio-temporal signals of the form $s(\boldsymbol{x}, t)$, where the 3D spatial variable is $\boldsymbol{x} = (x_1, x_2, x_3) \in \mathbb{R}^3$. Classical analysis of the IPR typically employs Fourier frequency-domain methods wherein all signals are assumed to be quasi-monochromatic (QMC) and can therefore be written in the form, $s(\boldsymbol{x}, t) = M(\boldsymbol{x}, t) \exp\left(j\bar{\omega}\boldsymbol{x}^T\right) \exp\left(j\omega_{t_0} t\right)$, $\bar{\omega} = \left(\omega_{x_1}, \omega_{x_2}, \omega_{x_3}\right)$ where ω_{t_0} is the constant temporal frequency and $\bar{\omega}$ is the 3D spatial frequency [1] [2] [3]. QMC-based analysis is, the steady-state periodic spatio-temporal frequency response and thereby does not directly reveal the dynamic (i.e., temporally transient) behavior of the IPR.

Although the complex exponential term $\exp\left(j\omega_{t_0} t\right)$ is implied, it is conveniently factored out of the QMC-based Fourier transfer function expressions [1] [2] [3], *allowing analysis to proceed by algebraic manipulations of spatial-frequency signal functions* of the form $M(\boldsymbol{x}) \exp\left(j\bar{\omega}\boldsymbol{x}^T\right)$, thereby characterizing the complete IPR system in terms of the 3D distribution $M(\boldsymbol{x})$ of *spatial* frequencies at the given constant temporal QMC frequency.

For the general case of propagating non-QMC PW signals $s_{AP}(ct)$ on the aperture, the following four analytical steps are necessary for full dynamic analysis:

1) Obtain the 1D Fourier transform $S_{AP}(j\omega_{ct})$ of $s_{AP}(ct)$.
2) Determine the 4D frequency-domain Fourier transfer function $H\left(j\omega_{x_1}, j\omega_{x_2}, j\omega_{x_3}, j\omega_{ct}\right)$ *from aperture disc to focal plane*. This transfer function must be valid over the relevant bandwidth of $S_{AP}(j\omega_{ct})$ and simplifies to a 2D transfer function $H(j\omega_r, j\omega_{ct})$ for the on-axis IPR case, where $\omega_r = \sqrt{\omega_{x_1}^2 + \omega_{x_2}^2}$.
3) Evaluate the 2D Fourier transform of the desired 2D spatio-temporal signal on the focal plane as the product $R_{fp}(j\omega_r, j\omega_{ct}) = S_{AP}(j\omega_{ct}) H(j\omega_r, j\omega_{ct})$.
4) Nontrivially, determine the 2D inverse Fourier transform $r_{fp}(x_r, ct) = \Im^{-2}\left[R_{fp}(j\omega_r, j\omega_{ct})\right]$ to yield the desired focal-plane dynamic response $r_{fp}(x_r, ct)$.

The above QMC-based process does not lend itself to closed-form algebraic spatio-temporal solutions for dynamic responses $r_{fp}(x_r, ct)$, nor does it lead to explanations or predictions of the dynamic behavior of the IPR. Dynamic analysis is almost always carried out numerically. Clearly, for the off-axis case, circular spatial symmetry is lost and therefore the above 2D Fourier transforms become 3D Fourier transforms over the spatio-temporal domain (x_1, x_2, ct).

APPENDIX B
THE FOCAL PLANE RESPONSE TO A DIRAC-PW APERTURE SIGNAL BY HUYGENS' INTEGRATION USING EXACT AND APPROXIMATE PATH DIFFERENCES

B.1 THE EXACT SOLUTION FOR $h_{fp}((x_1, x_2, 0), ct)$

Employing Huygens' principle to the elemental wavelets at each point P in Fig. 1, the focal plane response to a Dirac-PW in the aperture given by integration of the wavelets received from each elemental area in the aperture. Using polar coordinates (θ, φ) this yields the exact Huygens' solution for the focal plane response

$$h_{fp\_exact}(\boldsymbol{x}_r, \boldsymbol{ct}) = \int_{-\pi/2}^{\pi/2} \int_{-\theta_{MAX}}^{\theta_{MAX}} \frac{\cos(\bar{n}, \bar{r}_1)}{2\pi r_1 c} \times r_0^2 \delta\left(ct - \Delta_l(\boldsymbol{x}_r)\right) |\sin\theta| \, d\theta d\varphi \theta_{MAX} \leq \pi/2$$

where $\theta_{MAX} = \tan^{-1}\left(\frac{8FD}{16F^2 - D^2}\right)$ and therefore $F \geq D/4$ (B.1)

Evaluating this integral requires that the path lengths in the integrand be determined in terms of $(x_r, F, D, \theta, \varphi, c)$. From the geometry of Fig. 1, it can be shown that,

$$r_0 = 2F/(1 + \cos\theta) \tag{B.2}$$

and

$$r_1 = r_0 \sqrt{1 - \frac{2x_r \sin\theta \cos\varphi}{r_0} + \frac{x_r^2}{r_0^2}} \tag{B.3}$$

where

$$\theta = \sin^{-1}(r/r_0) \tag{B.4}$$

The exact path length difference from P to a point Q (see Fig. 1) on the focal plane at distance x_r from the focal point is given by,

$$\Delta_l(x_r) \equiv r_1 - r_0 = r_0 \left(\sqrt{1 - \frac{2x_r \sin\theta \cos\varphi}{r_0} + \frac{x_r^2}{r_0^2}} - 1 \right) \tag{B.5}$$

Substituting (B.2) and (B.3) in (B.5) yields the exact path difference

$$\Delta_l(x_r) = \frac{2F}{1 + \cos\theta} \left(\sqrt{1 - \frac{2x_r \sin\theta \cos\varphi}{\left(\frac{2F}{1+\cos\theta}\right)} + \frac{x_r^2}{\left(\frac{2F}{1+\cos\theta}\right)^2}} - 1 \right) \tag{B.6}$$

The following first order and second-order approximations approximate the above square root in terms of its Taylor series. It can be shown that the so-called obliquity term in (B.1) is given by (B.7), as shown at the bottom of the next page.

Substituting (B.6) and (B.7) in (B.1) yields the exact Huygens' expression $h_{fp\_exact}(x_r, F, D, ct)$. However, the

resulting integrand in (B.1) is far too complicated for algebraic integration and for understanding the dynamic behavior of the IPR. We have therefore numerically evaluated $h_{fp\_exact}\,(x_r, F, D, ct)$ using a MATLAB program that allows arbitrary temporal and spatial resolutions. For brevity, the numerical algorithm and the MATLAB program are omitted from this contribution although the results are used (in Fig. 4) as a comparative benchmark for estimating the accuracy of the first and second approximations h_{fp1}. and h_{fp2}.

B.2 THE FIRST ORDER AND SECOND ORDER APPROXIMATIONS

We make the widely employed assumption [1] that the obliquity term is approximated as follows.

$$\frac{cos\ (\bar{n}, \overline{r_1})}{2\pi r_1 c} \approx \frac{r_1}{2\pi c} \tag{B.8}$$

Following [4] [5] the well-known first order and the second order expressions for IPR path differences [1] [2] employ the first and second order terms of the Taylor Series expansion of the square root in (B.5). Accordingly, the *second-order approximation* assumes that

$$\left|\frac{x_r sin\,\theta cos\,\varphi}{r_0} + \frac{x_r^2}{2r_0^2}\right| \ll 1 \text{ and } cos\,\theta \approx 1 \tag{B.9}$$

yielding

$$\Delta_l\,(x_r) \approx -x_r sin\,\theta cos\,\varphi + \frac{x_r^2}{2F} \tag{B.10}$$

The *first-order approximation* imposes the yet more stringent assumption that

$$\frac{x_r}{4F}(1 + cos\,\theta) \ll |sin\,\theta cos\,\varphi| \tag{B.11}$$

yielding

$$\Delta_l\,(x_r) \approx -x_r sin\,\theta cos\,\varphi \tag{B.12}$$

APPENDIX C
DERIVATIONS OF FIRST-ORDER APPROXIMATION h_{fp1} AND SECOND-ORDER APPROXIMATION h_{fp2}

Substituting (B.8) in (B.1) yields

$$h_{fp1}\,(x_r, ct) = \int_{-\pi/2}^{pi/2}\int_{-\theta_{MAX}}^{\theta_{MAX}} \delta\,(ct + x_r sin\,\theta cos\,\varphi) \times |sin\,\theta|\,d\theta d\varphi \tag{C.1}$$

C.1 DERIVATION OF h_{fp1}

The inner integral of (C.1) cannot be performed directly over θ. To proceed we follow [4] [5] [13] to yield the equivalent relation

$$\delta\,(ctCx_r sin\,\theta cos\,\varphi) = \frac{\delta\left(\theta - sin^{-1}\left(\frac{bmct}{x_r cos\,\varphi}\right)\right)}{\sqrt{x_r^2 cos^2\varphi - (ct)^2}} \tag{C.2}$$

Substituting (C.2) into the inner integral of (C.1) yields the equivalent inner integral

$$\begin{aligned}\int_{-\theta_{MAX}}^{\theta_{MAX}} |sin\,\theta|\,\frac{\delta\left(\theta - \sin^{-1}\left(\frac{-ct}{x_r cos\,\varphi}\right)\right)}{\sqrt{x_r^2 cos^2\varphi - (ct)^2}} d\theta \\ = \left[\frac{|ct|}{x_r cos\,\varphi\sqrt{x_r^2 cos^2\varphi - (ct)^2}} u \right. \\ \left. \times \left(\theta - sin^{-1}\left(\frac{-ct}{x_r cos\,\varphi}\right)\right)\right]_{-\theta_{MAX}}^{\theta_{MAX}} \\ = \begin{cases} \dfrac{|ct|}{x_r cos\varphi\sqrt{x_r^2 cos^2\varphi - (ct)^2}}, & |ct| < x_r sin\,\theta cos\,\varphi \\ 0, & otherwise \end{cases}\end{aligned} \tag{C.3}$$

where $u\,(.)$ is the unit step function. To proceed to the outer integral (over ψ from $-\pi$ to π) we employ the indefinite integral identity [14].

$$\int \frac{1}{cos\ (\varphi)\sqrt{acos^2\,(\varphi) - 1}} dx = tan^{-1}\left(\frac{sin\,(\varphi)}{a\,cos^2\,(\varphi) - 1}\right) + C \tag{C.4}$$

implying the corresponding definite integral relation

$$\begin{aligned}\int_{\varphi_1}^{\varphi_2} \frac{1}{cos\,(\varphi)\sqrt{a\,cos^2(\varphi) - 1}} dx \\ = tan^{-1}\left(\frac{sin\ (\varphi_2)}{a\,cos^2\,(\varphi_2) - 1}\right) \\ - tan^{-1}\left(\frac{sin\,(\varphi_1)}{a\,cos^2\,(\varphi_1) - 1}\right)\end{aligned} \tag{C.5}$$

Note that this identity is different and algebraically far simpler than the identity in [5, 4] *and thereby makes possible new simplified closed form approximate solutions for the focal plane response.* Substituting $a = (x_r/ct)^2$ in (C.5) and substituting the result into (C.1) yields, after considerable algebraic manipulation,

$$h_{fp1}\,(x_r, ct) = \frac{1}{x_r}\int_{-cos^{-1}(ct/x_r sin\,\theta_{MAX})}^{cos^{-1}(ct/x_r sin\,\theta_{MAX})} \times \frac{1}{x_r cos\,\varphi\sqrt{x_r^2 cos^2\varphi - (ct)^2}} d\varphi \tag{C.6}$$

$$r_0^2 \frac{cos\ (\bar{n}, \overline{r_1})}{2\pi r_1 c} = \frac{2F^2\,(2F sin\,\theta tan(\theta/2) + 2F cos\,\theta - x_r sin\,\theta cos\,\varphi)}{\pi c(1 + cos\,\theta)\left(4F^2 - 4F x_r sin\,\theta cos\,\varphi(1 + cos\,\theta) + x_r^2(1 + cos\,\theta)^2\right)\sqrt{1 + tan^2(\theta/2)}} \tag{B.7}$$

Combining (C.6) and (C.5) yields, after further algebraic manipulation and simplification,

$$h_{fp1}(x_r, ct) = \begin{cases} \frac{2}{x_r}\tan^{-1}\left(\sqrt{1-\left(\frac{ct}{x_r sin\,\theta_{MAX}}\right)^2}\, tan\theta_{MAX}\right), \\ \qquad |ct| < x_r sin\,\theta_{MAX} \\ 0, \\ \qquad otherwise \end{cases} \tag{C.7}$$

and using θ_{MAX} from B.1 leads to

$$h_{fp1}(x_r, ct) = \begin{cases} \frac{2}{x_r}\tan^{-1}\left(\sqrt{1-\left(\frac{ct}{x_r sin\,\theta_{MAX}}\right)^2}\, \frac{8}{16\left(\frac{F}{D}\right)-\left(\frac{D}{F}\right)}\right), \\ \qquad |ct| < x_r sin\,\theta_{MAX}, \quad F \geq D/4 \\ 0, \\ \qquad otherwise \end{cases} \tag{C.8}$$

The ROS and shape of $h_{fp1}(x_r, ct)$are determined by the Dynamic Generating Function given by:

$$\Psi(x_r, t) = \sqrt{\left(1-\left(\frac{ct}{x_r sin\ (\theta_{max})}\right)^2\right)} \qquad 0 < \Psi(x_r, t) < 1 \tag{C.9}$$

The more complicated expression in [4] [5] yields the same ROS.

C.1 DERIVATION OF h_{fp2}

Comparing (B.10) and (B.12), the second-order path difference approximation contains the additional term $x_r^2/2F$, representing an additional time delay of $x_r^2/2Fc$. Consequently, the above analysis for h_{fp1} leading to (C.7), can be repeated but with this additional delay term to yield the simple relation that

$$h_{fb2}(x_r, c_t) \approx h_{fp1}\left(x_r, c_t - \frac{x_r^2}{2F}\right) \tag{C.10}$$

ACKNOWLEDGMENT

The authors acknowledge the significant contributions of the late Naeni Mehdi, M.Sc., Department of Electrical and Computer Engineering, University of Calgary.

REFERENCES

[1] J. W. M. Baars, *The Paraboloidal Reflector Antenna in Radio Astronomy and Communication: Theory and Practice*, 1st ed., New York, NY, USA: Springer-Verlag, 2007.
[2] M. Born and E. Wolf, *Principles of Optics: Electromagnetic Theory of Propagation, Interference and Diffraction of Light*, 7th ed. Cambridge, U.K.: Cambridge Univ. Press, 1999.
[3] J. W. Goodman, *Introduction to Fourier Optics*, 4th ed. New York, NY, USA: W. H. Freeman Company, 2017.
[4] M. A. Naeini, *Design of Variable Fractional Delay Farrow Filters for Radio Astronomy Application and 3D Space-Time Impulse Response Field of the Parabolic Reflector in the Focal Plane*. Calgary, AB, Canada: Univ. Calgary, 2011.
[5] M. A. Naeini and L. T. Bruton, "The 3D on-axis space-time scalar impulse response field of the parabolic reflector in the focal plane," in *Proc. IEEE Pacific Rim Conf. Commun., Comput. Signal Process.*, Victoria, BC, Canada, Aug. 2011, pp. 394–398.
[6] S. P. Skullcin and V. I. Turchin, "Transient field calculation of aperture antennas," *IEEE Trans. Antennas Propag.*, vol. 47, no. 5, pp. 929–932, May 1999.
[7] R. D. Oliveira and M. Helier, "Closed-form expressions of the axial step and impulse responses of a parabolic reflector antenna," *IEEE Trans. Antennas Propag.*, vol. 55, no. 4, pp. 1030–1037, Apr. 2007.
[8] R. de Oliveira and M. Helier, "Closed-form expressions of the axial prompt responses of a defocused parabolic reflector antenna," *IEEE Trans. Antennas Propag.*, vol. 57, no. 11, pp. 3685–3688, Nov. 2009.
[9] R. de Oliveira and M. Helier, "Time response of a parabolic reflector antenna to a generalized Gaussian pulse," in *Proc. 11th Int. Symp. Antenna Technol. Appl. Electromagn. [ANTEM]*, Jun. 2005, pp. 1–4.
[10] S. P. Skulkin, N. A. Lysenko, G. K. Uskov, and A. M. Bobreshov, "Formulas for antenna patterns in time domain and for the primitive impulse response function of linearly polarized field of plane aperture," *IEEE Antennas Wireless Propag. Lett.*, vol. 19, no. 9, pp. 1516–1520, Sep. 2020.
[11] R. T. Schilizzi, P. E. Dewdney, and J. W. Lazio, "The square kilometre array," in *SPIE Proceedings*, vol. 7733. San Diego, CA, USA: Ground-based and Airborne Telescopes III, Jul. 2010.
[12] T. S. Organization. *SKA Brochure, Posters and Infographics*. Accessed: Mar. 16, 2021. [Online]. Available: https://www.skatelescope.org/wp-content/uploads/2021/02/SKAO-Prospectus-2021.pdf
[13] E. W. Weisstein. *Delta Function, MathWorld–A Wolfram Web Resource*. Accessed: Mar. 16, 2021. [Online]. Available: https://mathworld.wolfram.com/DeltaFunction.html
[14] *WolframAlpha ExamplesIntegrals*. Accessed: Mar. 16, 2021. [Online]. Available: https://www.wolframalpha.com/examples/mathematics/calculus-and-analysis/integrals/

LEONARD T. BRUTON (Life Fellow, IEEE) has served as the Dean of engineering and the Vice-President (research) with the University of Calgary and the founding Dean of engineering with the University of Victoria, Canada. He is currently an Emeritus Professor with the University of Calgary and an Adjunct Professor with the University of Victoria. His current research interests include the applications of multidimensional filters in such fields as video signal processing, radio astronomy, wireless beamforming, and light field depth—filtering for photography and video processing. He is a fellow of the Royal Society of Canada.

SANDUNI PREMARATNE (Graduate Student Member, IEEE) received the B.Sc. and M.Phil. degrees in electronic and telecommunication engineering from the University of Moratuwa, Sri Lanka, in 2016 and 2019, respectively. She is currently pursuing the Ph.D. degree with the Department of Electrical and Computer Engineering, University of Victoria, Canada. Her current research interest includes multidimensional digital filters for light field processing.

PANAJOTIS AGATHOKLIS (Life Senior Member, IEEE) received the Dipl.Ing. degree in electrical engineering and the Dr.Sc.Tech. degree from the Swiss Federal Institute of Technology, Zürich, Switzerland, in 1975 and 1980, respectively.

He is currently a Professor with the Department of Electrical and Computer Engineering, University of Victoria, BC, Canada. His research interests include control, digital signal processing, and their applications. He worked on stability of multidimensional systems, space-time processing, signal processing in the gradient domain, applications of DSP in optical and radio astronomy, and processing of light fields.